Regular Paper

A Study on Distributions of Boron Ions Implanted by Using B and BF$_2$ Dual Implantations in Silicon

Won-Chae Jung[†]
Department of Electronic Engineering, Kyonggi University, Suwon 440-760, Korea

For the fabrication of PMOS and integrated semiconductor devices, B, BF$_2$ and dual elements with B and BF$_2$ can be implanted in silicon. 15 keV B ions were implanted in silicon at 7° wafer tilt and a dose of 3.0×10^{16} cm^{-2}. 67 keV BF$_2$ ions were implanted in silicon at 7° wafer tilt and a dose of 3.0×10^{15} cm^{-2}. For dual implantations, 67 keV BF$_2$ and 15 keV B were carried out with two implantations with dose of 1.5×10^{15} cm^{-2} instead of 3.0×10^{15} cm^{-2}, respectively. For the electrical activation, the implanted samples were annealed with rapid thermal annealing at 1,050°C for 30 seconds. The implanted profiles were characterized by using secondary ion mass spectrometry in order to measure profiles. The implanted and annealed results show that concentration profiles for the BF$_2^+$ implant are shallower than those for a single B$^+$ and dual (B$^+$ and BF$_2^+$) implants in silicon. This effect was caused by the presence of fluorine which traps interstitial silicon and BF$_2^+$ implants have lower diffusion effect than a single and dual implantation cases. For the fabricated diodes, current-voltage (I-V) and capacitance-voltage (C-V) were also measured with HP curve tracer and C-V plotter. Electrical measurements showed that the dual implant had the best result in comparison with the other two cases for the turn on voltage characteristics.

Keywords: B, BF$_2$, F, Dual implantations, Secondary ion mass spectrometry, Computer simulation, Current-voltage, Capacitance-voltage

1. INTRODUCTION

For the fabrication of complementary metal-oxide semiconductor (CMOS) devices, the source and drain regions can be formed by using BF$_2$, B, P and implantations for p$^+$ doping [1-6]. For ultra-shallow junctions, BF$_2$ impurities are implanted instead of B, and the implanted wafers are annealed for the electrical activation in a N$_2$ ambient. As device sizes shrink, the accurate control of channel length and depth is very important in the CMOS process. Nowadays, the effects of transient enhanced diffusion and activation mechanisms of implanted ions are also investigated extensively [1, 2]. However, some effects such as ion cluster-formations and diffusions are still not fully explained. The distributions of implanted impurities were analyzed by using integrated circuits and electronics group computerized remedial education and mastering (ICECREM) of the analytical simulation [7-9], and the results were compared with secondary ion mass spectrometry (SIMS) data. UT-Marlowe [10] was used as a Monte Carlo simulation tools [11-14] for one-dimensional profiles in amorphous and crystalline silicon. The calculated moments of UT-Marlowe data were inserted into an analytical model in order to get diffusion profiles. In the simulation, all annealing processes used the analytical model [7-9] with the proper diffusion coefficients. The output data of the analytical model closely matched the measured SIMS data after furnace annealing. For the calculation of moments in the vertical direction, the following equations were used.

$$C(x) = C_{dose} \cdot f(x) \tag{1}$$

where C$_{dose}$ is the implanted dose, C(x) is the concentrations as a function of the depth x, and $f(x)$ is a normalized distribution function. The four moments are defined as

$$R_P = \int_0^\infty x \cdot f(x) \tag{2}$$

[†] Author to whom all correspondence should be addressed:
E-mail: wcjung@kyonggi.ac.kr

Trans. Electr. Electron. Mater. 11(3) 120 (2010): W.-C. Jung

121

$$\Delta R_p = \sqrt{\int_0^\infty (x - R_p)^2 \cdot f(x)dx} \tag{3}$$

$$\gamma = \frac{\int_0^\infty (x - R_p)^3 \cdot f(x)dx}{\Delta R_p^{\,3}} \tag{4}$$

$$\beta = \frac{\int_0^\infty (x - R_p)^4 \cdot f(x)dx}{\Delta R_p^{\,4}} \tag{5}$$

where the first moment R_p (projected average range) is the average range under normal implantation, the second moment ΔR_p (standard deviation) represents the profile width, the third moment γ (skewness) indicates the asymmetry of the profile, and the fourth moment β (kurtosis) represents the extent of profile sharpness in the peak-concentration area. A gaussian profile has only two parameters due to symmetry, and the equation can be expressed as,

$$C(x) = \frac{C_{dose}}{\sqrt{2\pi}\Delta R_p} \exp\left(-\frac{1}{2}\left[\frac{x - \Delta R_p}{\Delta R_p}\right]^2\right) \tag{6}$$

The projected average range (R_p) of the Gaussian profile is located near the peak concentration.

The equation of concentration distribution after annealing is $\Delta R_p = \sqrt{\left(\Delta R_p^{\,2} + 2Dt\right)}$ due to diffusion effects. The Gaussian profile is generally not adequate to express asymmetry profiles caused for B, BF_2 and dual (B and BF_2) implanted silicon.
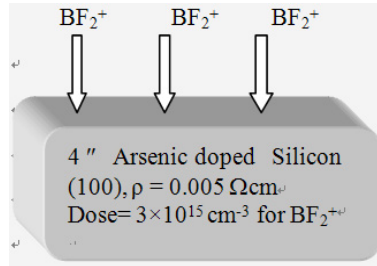
2. EXPERIMENTS OF B, BF₂, AND DUAL IMPLANTATIONS

In this experiment, (100) arsenic-doped n type, silicon wafers with values with ρ of 0.005 $\Omega\cdot$cm, were used. The concentration of silicon substrate was about 1×10^{19} cm^{-3}.

For the p type doping, B, BF_2, dual (B and BF_2) ions were implanted in silicon wafers. For the doping of source and drain formation for CMOS fabrication, three different implantations with the same doses were carried out into silicon substrate by using a VARIAN medium current implanter. Before the implantation, the accelerated energies were calculated by applying the mass-ratio of elements for the same range. First, 15 keV ^{11}B ions were implanted in silicon at 7° wafer tilt and a dose of 3.0×10^{15} cm^{-2}. Second, 67 keV ^{49}BF$_2$ ions were implanted in silicon at 7° wafer tilt and a dose of 3.0×10^{15} cm^{-2}. Third, dual (B and BF_2) implantations were carried out. Namely, 67 keV ^{49}BF$_2$ ions were implanted in silicon at 7° wafer tilt and a dose of 1.5×10^{15} cm^{-2}. Also, 15 keV B ions were implanted in silicon at 7° wafer tilt and a dose of 1.5×10^{15} cm^{-2}. Three different implantations were carried out at 7° wafer tilt to avoid the channeling effect in Fig. 1.

For the electrical activation, annealing processes with rapid thermal annealing (RTA) were carried out in a N_2 gas ambient at 1,050°C for 30 seconds. For the three implantation cases, the measured boron profiles were compared as depicted in Fig. 1. For the fabrication of three different diodes, the native oxides in implanted samples were etched off by dipping in a buffered oxide etchant (BOE) solution. After removal of the native oxide, the implanted wafers were coated with aluminum (Al) on the surface by using sputtering to form electrode material with thickness of 6,000 Å. For the alloying process of good electrical contact,
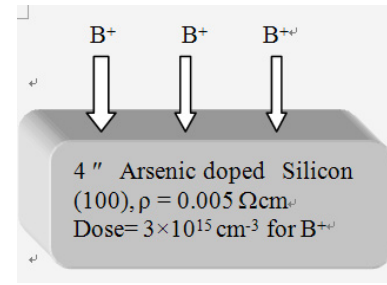
(a) B⁺ implanted p-n junction

(b) BF₂⁺ implanted p-n junction
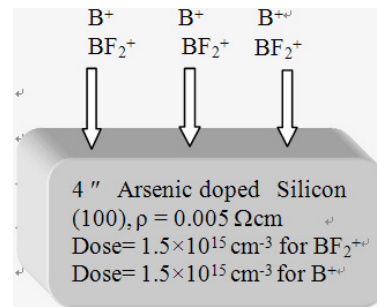
(c) p-n junction by using dual implantation

Fig. 1. Three different formations of p-n junctions fabricated by using B⁺, BF₂⁺ and dual implantations.

the implanted wafers were annealed in the 450°C for 30 minutes under N_2 ambient gas by using electrical furnace. The fabricated diode was scribed and cut off as a size of 5 mm × 5 mm by using a dicing saw. Current-voltage (I-V) and capacitance-voltage (C-V) characteristics of the diode were measured. The measured data of three different diodes are compared with one another in Figs. 12 and 13, respectively.

3. RESULTS AND DISCUSSION

### 3.1 Comparisons with measured and simulated data

The profiles of implanted boron in silicon were measured by using SIMS. The experimental conditions for SIMS are shown in Table. 1.

The implanted profiles were measured by using CAMECA IMS 7f SIMS. The profile of boron implanted silicon is deeper than the other two cases. On the other side, the boron profile measured by using BF_2 implantation in silicon is shallower than a direct B implantation, because ^{49}BF$_2$ is 4.46 times heavier than ^{11}B and the range implanted of boron in ^{49}BF$_2$ is shorter than that of ^{11}B. When ^{49}BF$_2$ is implanted, ^{11}B⁺ and ^{38}F$_2^+$ ions are dissociated and the range in ^{19}F ions is deeper in the bulk silicon than in ^{11}B because of the lower electronic stopping power of ^{19}F. The profiles at the peak concentration have very similar shapes.

Table 1. Experimental conditions for SIMS measurements of ^{11}B profiles.

Primary ions	O_2^+
Impact energy	5,000 eV
Source extraction voltage	10,000 V
Sample extraction voltage	5,000 V
Incidence angle	46.2°
Primary Beam intensity	100 nA
Mass resolution	400
Raster size	200 μm
Analyzed area size	33 μm
Vacuum in analysis chamber	6.680e-10 torr

SIMS: secondary ion mass spectrometry.
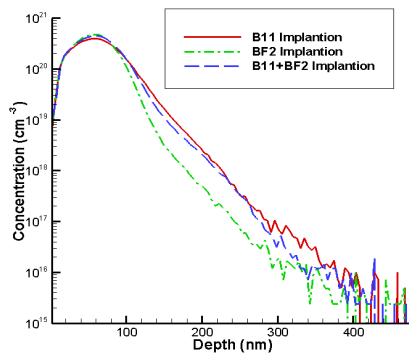
Fig. 2. Implanted boron profiles measured using secondary ion mass spectrometry.

Nevertheless, the profiles at the tail regions are different from the three implanted samples. This effect occurs because fluorine can trap interstitial silicon and cause the abnormal boron distribution from the interstitial silicon, defects, and vacancy distributions. For the explanation of amorphized layers with increasing implant doses, the defects dynamics were used citations from the published papers [15] instead of different experimental conditions, which were as follows. BF_2^+ ions were implanted with 50-keV energy at 0° into SiO_2(200 Å)/Si. The TEM (transmission electron micrograph) results of the specimens implanted with dose higher than 5×10^{14} cm^{-2} showed that the thickness of amorphized layers with increasing implant doses. The thickness of amorphized layers were measured to be 200, 400, and 550 Å for the specimens implanted with 1×10^{15} cm^{-2}, 5×10^{15} cm^{-2}, and 1×10^{16} cm^{-2}, respectively.

Boron ions were implanted in silicon at a 7° tilt angle to avoid channeling effects and the B profiles measured by using SIMS are shown in Fig. 2.

B ions were implanted in silicon at a 7° tilt angle to avoid channeling effects and the measured SIMS and UT-Marlowe simulation data are compared in Fig. 4. Although the avoidance of channeling effects are considered at a 7° tilting condition, the channeling effects is still shown in Figs. 3-5 from the SIMS data. The UT-Marlowe program can be used to verify implanted profiles in the crystalline silicon. The data of the UT-Marlowe simulation matches the SIMS data relatively well. For good statistical resolutions of profiles in crystalline silicon, 100,000 ions were selected for the UT-Marlowe simulation.

BF_2 ions were implanted in silicon at a 7° tilt angle and compared between measured SIMS and UT-Marlowe simulation data in Fig. 4. The shape of the B profile is smaller than in other cases due to dissociation effects of B and F ions and fluorine can trap interstitial silicon.

The dual (BF_2 and B) ions were implanted in silicon at a 7° tilt angle for the boron profiles and compared between measured
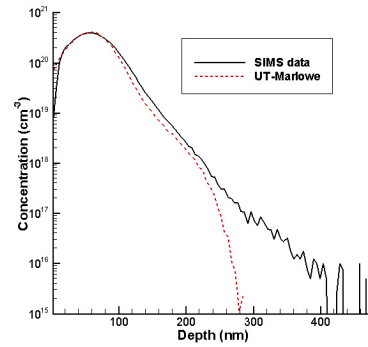
Fig. 3. Comparison of ^{11}B implanted profiles with secondary ion mass spectrometry (SIMS) and simulated data for the boron profiles.
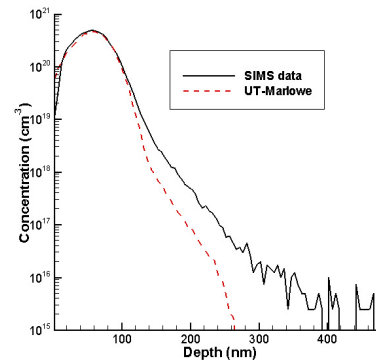
Fig. 4. Comparison of BF_2 implanted profiles with secondary ion mass spectrometry (SIMS) and simulated data for the boron profiles.
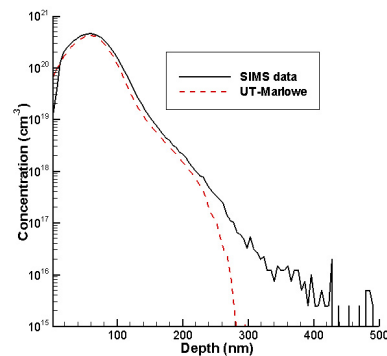
Fig. 5. Comparison of dual (BF_2 and B) implanted profiles with secondary ion mass spectrometry (SIMS) and simulated data for the boron profiles.

SIMS and UT-Marlowe simulation data in Fig. 5.

The implanted samples were annealed at 1050°C for 30 seconds under N_2 ambient gas by using RTA. After the annealing process at 1,050°C for 30 seconds under N_2 ambient gas, the boron profile in the BF_2 implantation is shallower than in the corresponding boron profiles of B implantation because of retarded diffusion due to fluorine. The boron profiles of dual implantation shows the middle distribution between BF_2 and B implantations except for peak concentration. The calculated data of implanted and annealed B are shown in Tables 2 and 3.

Implanted boron profiles were measured by using CAMECA IMS 7f SIMS and were compared with simulated data using the UT-Marlowe simulation tool. Three different implantations were carried out by using source ions of B, BF_2, and dual (B and BF_2). After the annealing process of the implanted samples at 1050°C

Table 2. The calculated B moments of SIMS and simulated data of UT-Marlowe program.

Model	Measured of SIMS data			Simulated data of UT-Marlowe		
Data	B	BF_2	Dual	B	BF_2	Dual
R_p(nm)	64.2	57.4	61.7	59.7	55.6	58.6
ΔR_p(nm)	31.8	25.2	29.5	30.1	24.5	28.8
γ	0.98	0.62	0.94	0.72	0.11	0.71
β	5.56	5.05	5.8	4.62	2.94	4.8

SIMS: secondary ion mass spectrometry.

Table 3. The calculated B moments of annealed SIMS and simulated data of ICECREM program after annealing.

Model	Measured of SIMS data			Simulated results of ICECREM data by using SIMS data		
Data	B	BF_2	Dual	B	BF_2	Dual
R_p(nm)	85.9	88.8	92.7	80.4	82	85.2
ΔR_p(nm)	47.3	49.0	50	46.1	47	48.6
γ	0.53	0.44	0.4	0.27	0.32	0.39
β	2.74	2.45	2.41	2.11	2.23	2.3

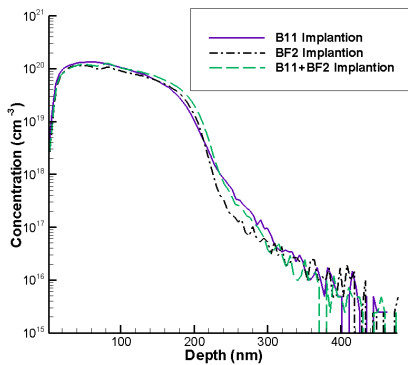SIMS: secondary ion mass spectrometry.

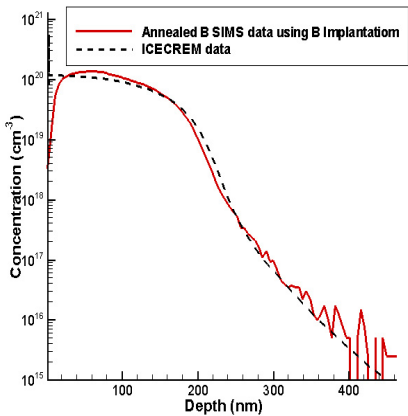Fig. 6. Annealed boron (^{11}B) profiles measured by using secondary ion mass spectrometry.

Fig. 7. Annealed boron (^{11}B) secondary ion mass spectrometry (SIMS) data by using B implantation.

Fig. 8. Annealed boron (^{11}B) secondary ion mass spectrometry (SIMS) data by using BF_2 Implantation.
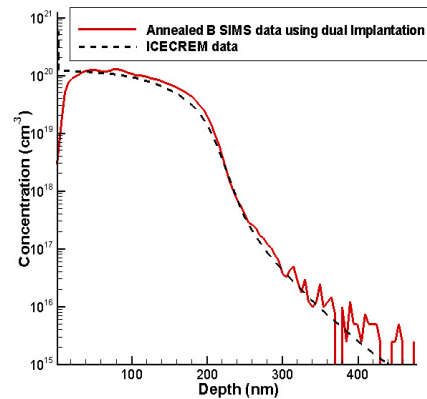
Fig. 9. Annealed boron (^{11}B) secondary ion mass spectrometry (SIMS) data by using dual (BF_2+B) Implantations.

for 30 seconds in N_2 gas by using RTA, the annealed boron profiles from SIMS are compared with one another in Fig. 6.

The peak concentrations are shown around 1.3×10^{20} cm^{-3} in Fig. 6. The measured SIMS data in Fig. 2 are simulated for the diffused profiles by using ICECREM in Fig. 7.

The peak concentrations are shown around 1.97×10^{20} cm^{-3} in Fig. 7. It can be explained because of different diffusion coeffi-

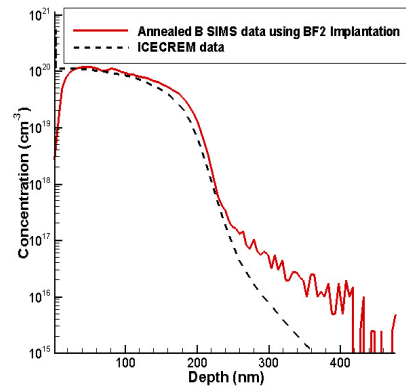cients and a little bit of out-diffusion of boron toward the surface in real samples. In any case, the diffusion mechanisms show very similar results between Figs. 6 and 7. After the annealing process, the B profile implanted by using BF_2 is shown as the shallowest profile due to the diffusion retarding effect of fluorine in Fig. 8. The profile of the dual implanted case is shown in the middle curve between the B and BF_2 cases in Fig. 6. The annealed SIMS profiles are each compared with simulated data in Figs. 7- 9, respectively.

The implanted and annealed F profiles were measured using SIMS in Fig. 10.

The F profile implanted by using BF_2 is shown as a solid line. On the other hand, the F profile implanted by using dual implantations is shown as a dash-dot-dot line, and has lower peak intensity due to a half dose of fluorine. The published TEM results showed that the dislocations have climbed towards the wafer surface as the length of anneal increased while F profiles reveal that 75% of implanted fluorine has out-diffused after 30 seconds RTA anneal at 1,100°C [16]. Fluorine out-diffused but is trapped at residual implantation damage which consists of dislocation loops [16]. After the 30 seconds RTA anneal at 1,050°C, F profiles are measured by using SIMS. Two fluorine peaks are detected at the depth of 53.13 and 100.13 nm for BF_2 implanted wafer and 35.34 and 67.06 nm for the dual implanted sample, respectively in Fig. 10.

In the experiments, F profiles reveal that 68.2% for the BF_2 and 34% for the dual case of implanted fluorine have out-diffused after 30 seconds RTA anneal at 1,050°C. Because this result showed originally different fluorine dose ratio caused between the BF_2 and the dual implantations.
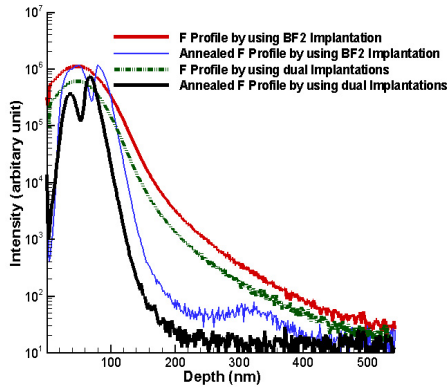
Fig. 10. Implanted and annealed F profiles in silicon by using secondary ion mass spectrometry.
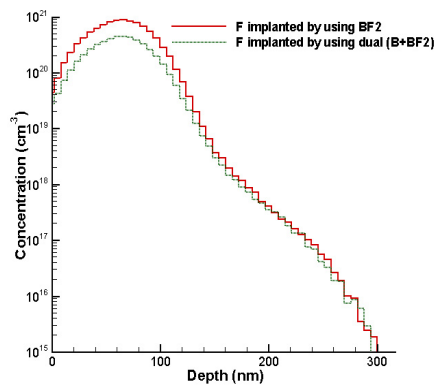

Fig. 11. Simulated F profiles in BF$_2$ and dual implanted silicon using UT-Marlowe .

Table 4. Experimental conditions for SIMS measurements of ^{19}F profiles.

Primary ions	Cs$^+$
Impact energy	15,000 eV
Source extraction voltage	10,000 V
Sample extraction voltage	-5,000 V
Incidence angle	23.7°
Primary beam intensity	50 nA
Mass resolution	400
Raster size	200 μm
Analyzed area size	55 μm
Vacuum in analysis chamber	9.030e-10 torr

SIMS: secondary ion mass spectrometry.

The measurement conditions for F profiles by using SIMS are shown in Table 4.

The implanted fluorine profiles were measured by using SIMS in Fig. 10.

The simulated data from UT-Marlowe are shown in Fig. 11. The value of intensity of 10^6 in Fig. 10 corresponds to a concentration about 10^{21} in Fig. 11.The implanted F profiles are simulated by using UT-Marlowe tool in Fig. 11. The measured F profiles showed very similar forms to the simulated data, but the annealed F profiles are shown two peaks from the F behavior of fluorine diffusion from the bulk to surface because of saturation in the interstitial of silicon. The peak concentrations of the BF$_2$ case are greater than those of the dual implantations due to a higher F dose. The diffused F profiles could not be simulated due to trapping of interstitial silicon, and the movement of F from bulk to surface was not controllable for simulation because of different doses and diffused temperatures. After the annealing
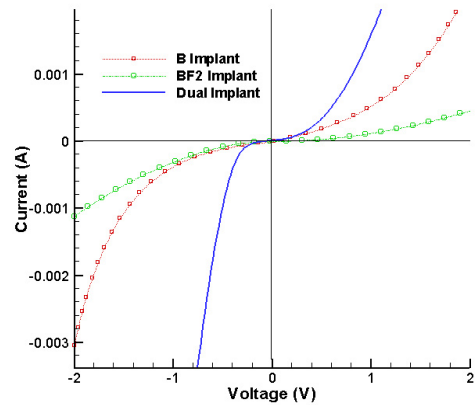

Fig. 12. Current -voltage characteristics of three p-n junction diodes.
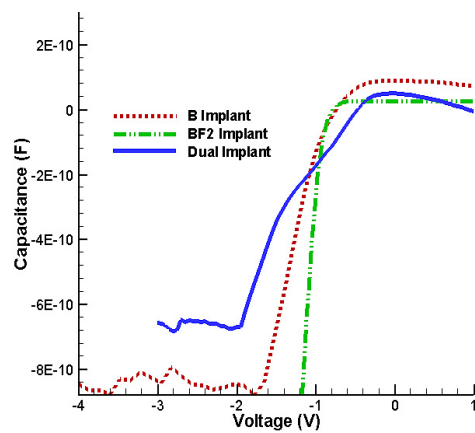

Fig. 13. Capacitance -voltage characteristics of three p-n junction diodes.

process, two peaks of the measured F have somewhat different forms between BF$_2$ and dual implanted cases due to different doses. Up to now, the diffusion mechanism of F in silicon was not clearly explained, and there was not an accurate theoretical model from the published research papers. From the different temperatures, an explanation and model of the annealed F profile must be developed in the future.

3.2 Electrical measurements for the fabricated diodes

The measurements of current and voltage are shown in Figs. 12 and 13, respectively.

The diode fabricated using BF$_2$ implantation has flat characteristics on the voltage axis. The diode fabricated using B implantation has steeper characteristics than the case of implanted BF$_2$. The diode fabricated using dual implantations showed the best turn on voltage characteristics of the three different diodes. Namely, turn-on voltages were 0.39 V for dual, 0.6 V for B, and 0.67 V for BF$_2$, respectively in Fig. 12. For the characteristic of breakdown voltages, the BF$_2$ implanted case is relatively the best result from three p-n junction diodes fabricated by using different implantations.

The C-V characteristics of the three different diodes are measured and compared by using the HP C-V plotter. The C-V characteristic of the BF$_2$ implanted diode changes rapidly from positive to negative voltage. From the three different diodes, the depletion layer in the BF$_2$ case shows the fastest control from positive to negative voltage. The change of capacitance of the BF$_2$

Trans. Electr. Electron. Mater. 11(3) 120 (2010): W.-C. Jung

125

case is more abrupt than that of other cases. It means the depletion width of BF_2 can be reacted faster than that of other cases from positive to negative voltage.

4. CONCLUSIONS

In the experiments, B, BF_2, and dual (B and BF_2) ions were implanted into n type silicon. For the electrical activation, the implanted wafers were annealed using RTA. The implanted and annealed SIMS profiles and the calculated range data were compared using UT-Marlowe and ICECREM simulation tools. They matched very well except channeling tail regions. The experimental results could be verified by the scaling of implanted ranges from different species and energies. For the formation of electrodes, the removal of native oxide was carried out using buffered oxide etchant (BOE) chemical treatments. Aluminums were coated onto the silicon by using sputtering technology. The implanted and annealed results show that concentration profiles for BF_2^+ implant are shallower than those for a single B^+ and dual (B^+ and BF_2^+) implants in silicon. This effect was caused by the presence of fluorine, which traps interstitial silicon, and BF_2^+ implant have a lower diffusion effect than a single and dual implantation cases. The fabricated diodes were investigated for the electrical measurements of I-V and C-V. The electrical characteristics of V_T (turn on voltage) using the dual implantations was the best result from among the three different diodes in Fig. 12. Therefore, the dual implantations for the formation of the P channel (P-MOS) can be used to improve the characteristics of the threshold voltage for the CMOS integrated circuits. The middle value of the C-V characteristics between B and BF_2 implantations are shown in the dual implantation in Fig. 13. The change of capacitance of the BF_2 case has a more abrupt shape than that of other cases. This means the depletion width of BF_2 can be reacted more quickly than that of other cases from the operations of positive to negative voltage. After the BF_2 and dual implantations, the SIMS profiles of F were matched very well with simulation data by using UT-Marlowe in Figs. 10 and 11. Nevertheless, the annealed F profiles showed two peaks and the diffusion mechanism was unexplainable and very complex for the trapping mechanism of interstitial silicon and out-diffusion toward the surface due to different temperatures.

REFERENCES

[1] W. C. Jung, J. KEEME, **15**, 289 (2002).
[2] W. C. Jung, J. Korean Phys. Soc. **46**, 1218 (2005).
[3] W. C. Jung and K. D. Lee, J. Korean Phys. Soc. **45**, 1078 (2004).
[4] R. G. Wilson, J. Appl. Phys. **54**, 6879 (1983) [DOI: 10.1063/1.331993].
[5] W. S. Yoo, T. Fukada, T. Setokubo, K. Aizawa, and T. Ohsawa, Jpn. J. Appl. Phys. **42**, 1123 (2003) [DOI: 10.1143/JJAP. 42.1123].
[6] A. Dusch, J. Marcon, K. Masmoudi, F. Olivie, M. Benzohra, K. Ketata, and M. Ketata, Mater. Sci. Eng. B **80**, 65 (2001) [DOI: 10.1016/S092-5107(00)00590-0].
[7] H. Ryssel and I. Ruge, "Ion Implantation", Wiley, New York, (1986) p. 125.
[8] L. Frey, S. Bogen, L. Gong, W. Jung, and H. Ryssel, Nucl. Instrum. Methods Phys. Res. Sect. B **62**, 410 (1992) [DOI: 10.1016/0168-583X(92)95267-U].
[9] L. Gong, S. Bogen, L. Frey, W. Jung, and H. Ryssel, Microelectron. Eng. **19**, 495 (1992) [DOI: 10.1016/0167-9317(92)90482-7].
[10] A. F. Tasch and S. K. Banerjee, Nucl. Instrum. Methods Phys. Res. Sect. B **112**, 177 (1996) [DOI: 10.1016/0168-583X(95)01246-X].
[11] U. Littmark and J. F. Ziegler, Phys. Rev. **23**, (1980) [DOI: 10.1103/PhysRevA.23.64].
[12] J. P. Biersack and J. F. Ziegler, "Ion Implantation Techniques", Springer-Verlag, Berlin, (1982) p. 281.
[13] T. E. Seidel, Nucl. Instrum. Methods Phys. Res. B **21**, 96 (1987).
[14] J. P. Biersack, Nucl. Instrum. Methods Phys. Res. B **35**, 205 (1988).
[15] M. C. Paek, O. J. Kwon, J. Y. Lee, and H. B. Im, J. Appl. Phys. **70**, 4176 (1991).
[16] C. W. Bates, Jr. , Appl. Phys. Lett. **45**, 1058 (1984).